Article

Visualization of Vascular Perfusion of Human Pancreatic Cancer Tissue in the CAM Model and Its Impact on Future Personalized Drug Testing

Andreas Ettner-Sitter [1,†], Agata Montagner [1,2,†], Jonas Kuenzel [1], Kathrin Brackmann [2], Maximilian Schäfer [3], Robert Schober [3], Florian Weber [4], Thiha Aung [1,5], Christina Hackl [2,‡] and Silke Haerteis [1,*,‡]

1   Institute for Molecular and Cellular Anatomy, University of Regensburg, 93053 Regensburg, Germany; andreas.ettner-sitter@ur.de (A.E.-S.); agata.montagner@ur.de (A.M.)
2   Department of Surgery, University Hospital Regensburg, 93053 Regensburg, Germany; christina.hackl@klinik.uni-regensburg.de (C.H.)
3   Institute for Digital Communications, Friedrich-Alexander-Universität Erlangen-Nürnberg, 91058 Erlangen, Germany
4   Institute of Pathology, University of Regensburg, 93053 Regensburg, Germany
5   Faculty of Applied Healthcare Science, Deggendorf Institute of Technology, 94469 Deggendorf, Germany
*   Correspondence: silke.haerteis@ur.de
†   These authors contributed equally to this work.
‡   These authors also contributed equally to this work.

Abstract: Although significant improvements have been made in the treatment of pancreatic cancer, its prognosis remains poor with an overall 5-year survival rate of less than 10%. New experimental approaches are necessary to develop novel therapeutics. In this study, the investigation of pancreatic cancer tissue growth in the chorioallantoic membrane (CAM) model and the subsequent use of indocyanine green (ICG) injections for the verification of intratumoral perfusion was conducted. ICG was injected into the CAM vasculature to visualize the perfusion of the tumor tissue. The presence of metastasis was investigated through PCR for the human-specific ALU element in the liver of the chicken embryo. Additionally, the usage of cryopreserved pancreatic tumors was established. Intratumoral perfusion of tumor tissue on the CAM was observed in recently obtained and cryopreserved tumors. ALU-PCR detected metastasis in the chick embryos' livers. After cryopreservation, the tissue was still vital, and the xenografts generated from these tumors resembled the histological features of the primary tumor. This methodology represents the proof of principle for intravenous drug testing of pancreatic cancer in the CAM model. The cryopreserved tumors can be used for testing novel therapeutics and can be integrated into the molecular tumor board, facilitating personalized tumor treatment.

Keywords: indocyanine green; pancreatic cancer; cryopreservation; CAM model; 3D in vivo tumor model

1. Introduction

Pancreatic ductal adenocarcinoma (PDAC) is the most common malignant neoplasm of the pancreas (80% of all pancreatic cancers), and it is characterized by aggressiveness, invasiveness, and resistance to chemotherapy [1]. According to the International Agency for Global Cancer Statistics, approximately 495,773 new cases of pancreatic cancer were diagnosed worldwide in 2020 [2]. Due to demographic changes and an increase in risk factors such as smoking, alcohol consumption, and obesity, the incidence is expected to increase in the future. PDAC is already the third leading cause of cancer-related death in the EU and is expected to be the second by 2030 [3–6]. The absence or non-specificity of symptoms and the unfavorable location of the pancreas complicate early detection and contribute to poor prognosis which is mainly due to early metastatic disease [7,8].

Intra-abdominal distant metastases are the most common cause of PDAC-related death [9]. In some cases, the formation of metastases is observed years after the primary surgery. Although circulating tumor cells have a brief half-life in peripheral blood, disseminated tumor cells can survive in the bone marrow niche dormant for even several years, then they can re-enter the bloodstream and, thus, may be the cause of distant metastasis [10–13]. However, surgery remains the only potentially curative option for PDAC, but a curative surgical approach is only possible in cases of locally confined tumors. Up to 80% of patients present themselves with tumors in advanced stages [1]. Patients with borderline resectable disease benefit from neoadjuvant chemotherapy and chemoradiation. For patients with locally advanced or metastatic disease, chemotherapy with FOLFIRINOX, gem-nabP, or gemcitabine + capecitabine +/− radiation is usually recommended [14,15]. Folfirinox is considered a very aggressive combination treatment, offering a median progression-free survival of six months for PDAC patients [16]. However, chemoresistance is one of the main causes of the poor outcome of pancreatic cancer [15,17].

The chorioallantoic membrane (CAM) model is regarded as a versatile tumor angiogenesis assay used to study multiple cancers [18–20]. The CAM is a highly vascularized extraembryonic membrane that forms between the 3rd and 10th day of embryonic development in fertilized chicken eggs [21]. Due to its immunodeficiency and its high density of blood vessels, this membrane is an excellent tumor angiogenesis model. Furthermore, this model enables the testing of potential therapeutics, monitoring of angiogenesis, and even the detection of possible metastases in the organs of the embryo [22]. The engrafted tumor tissue, as well as the CAM vessels, are directly accessible through a window that is cut into the eggshell. Moreover, a primary tumor can be cut into multiple small pieces and engrafted in multiple CAM models, allowing the possibility of replication. In this way, the heterogeneity of a tumor is taken into account and, if necessary, accidental therapeutic (mis)successes are avoided because drugs are tested for many different pieces of tumor cultivated on different CAMs. This opens an opportunity for direct testing of both conventional and novel molecular-targeted therapeutics [23,24].

To yield essential insights into the biology of PDAC to develop approaches for improved treatment options, the characterization of genetic alterations in PDAC is becoming more and more important. Molecular panel testing of resected tumor tissue is currently becoming an exceeding part of routine screening methods for many cancers, including PDAC patients. Usually, the molecular screening focuses on the most commonly mutated genes in PDAC: KRAS, TP53, SMAD4, and CDKN2A. KRASG12C inhibitors have shown an effect in G12C-mutated cancers and pan-RAS inhibitors are a less specific alternative for non-G12C-KRAS [25,26]. The results are then discussed in so-called interdisciplinary molecular tumor boards that identify promising new molecular targets in patients. Therapies targeting these new molecular targets are only utilized after resistance to conventional chemotherapy as they are costly and often involve off-label prescription [27]. Here, the CAM offers the opportunity to directly test novel molecular therapeutics in immediate comparison to standard chemotherapy within a time- and cost-efficient setting [28]. After surgical resection, the tumor tissue received from the patient can be either applied immediately to the CAM or frozen after the dissection for cryopreservation and later grafted onto the CAM. Cryopreservation allows for optimal timing of grafting, such as when waiting for the molecular tumor board's decision.

Testing of intravenously administered therapeutics in the CAM model requires anastomoses between tumor vessels and the blood circulation of the embryo. In this context, intravenously applied indocyanine green (ICG) could provide a method to visualize, monitor, and quantify intratumoral perfusion to determine whether administered therapeutics can reach the target tissue. Due to its ability to fluorescence when stimulated with light in the infrared wavelength range, ICG is known for its use in liver function analysis [29], lymph node imaging [30], and intraoperative tumor tissue visualization [31]. Based on its composition, it interacts with macromolecular serum proteins such as albumin, known to be enriched in most cancers [32]. In clinical use, chemotherapy is applied to patients intra-

venously, as we also perform in our setting. Alternatively, therapeutic agents can also be administered topically, although this type of treatment is less targeted. With topical administration, the therapeutic agent does not remain on the graft but spreads to the surrounding CAM. Moreover, the therapeutic agent can only affect the upper layers, but not the deeper tissue layers and blood vessels of the tumor. Regarding this topic, Kue et al. found that the median lethal dose and the median survival dose of several FDA-approved chemotherapeutics injected into CAM vessels appeared to moderately correlate with intravenous and intraperitoneal application doses for rodents [33]. Finally, since the blood volume increases during the development of the chick embryo, larger volumes can be injected at more advanced stages of embryo development [34]. Another important aspect of tumor biology is drug delivery. Studying the distribution of ICG inside the CAM model might be useful for analyzing and designing targeted drug delivery which enables therapeutics to be directly "delivered" and released at the target site [35]. However, complications such as their rapid systemic elimination, uptake by the reticuloendothelial system, and deposition in other tissues might occur [36]. The following three aspects play an important role in the development of new drug delivery systems: target detection (methods for the localization of diseased cells), drug propagation (models for the distribution of drug carriers/molecules in the circulatory system), and drug release (optimization of drug release profiles) [37–39].

In recent years, organoids have become increasingly relevant as a promising tool for basic research and drug research. They are utilized in a wide spectrum of applications, from oncology and regenerative medicine to disease modeling and drug screening. As 3D structures, they enable more precise monitoring of processes in a more physiologically relevant environment and therefore open up new possibilities compared with previously used monolayer cultures [40]. Vascularized kidney, brain, and cardiac pre-vascularized organoids have already been successfully grown on the CAM [41,42]. The further establishment of the cultivation of organoids on the CAM could replace several of the in vivo models used to date, including various species of experimental animals, and enable research in tumor biology without the use of additional laboratory animals.

Tumor metastasis is currently diagnosed clinically, by medical imaging and serum marker assays, but the effectiveness regarding early tumor detection is very limited. Identification at a very early stage might have a significant impact on the therapy and subsequently the outcome. Therefore, we performed a polymerase chain reaction (PCR) using Alu sequences as a first promising target for detecting metastases in the chick's organs. Alu elements, such as Alu-247 and Alu-155, known for their role in metastasis [43], are retrotransposons distributed throughout the human genome and found only in primates [44]. Hence, these target sequences are used for the identification of human tumor cells.

Furthermore, this study aims to establish near-infrared imaging as a standardized method in the well-described CAM model to confirm the connection of human tissue to the circulating system of the embryo and to visualize and quantify intratumoral perfusion. These results could serve as a basis for the investigation of intravenously administered therapeutics and their effects in further projects. Moreover, the CAM model can also be used to analyze the process of metastasis to gain a more in-depth insight into tumor biology and new therapeutic targets.

2. Materials and Methods

2.1. Study Participants

PDAC tissue samples were collected from patients who had been diagnosed with PDAC and underwent surgical resection at the Department of Surgery of the University Hospital Regensburg. Patients who were eligible for surgery gave their informed consent to the research project before the surgery was performed, according to the ethical guidelines of the "World Medical Association Declaration of Helsinki—Ethical Principles for Medical Research Involving Human Subjects". Approval of the ethics committee of the University Hospital Regensburg was obtained (ethics approval number 20-1989-101).

2.2. CAM model

As previously described, chicken eggs were purchased from a local organic chicken farm and incubated at 37.8 °C, a pCO2 of 5%, and humidity calibrated to 63% [32–34]. First, an approximately 5 mm × 5 mm hole was cut into the eggshell using sterile scissors, followed by a second larger hole (1 cm × 1 cm) in the longitudinal side of the eggshell. The second window was enlarged on day 4 and the eggshell was sealed with Leukosilk® (BSN medical, Hamburg, Germany). Tumor tissue was cut into approximately 3 mm × 3 mm × 1 mm pieces and grafted onto the CAM (Figure 1). A part of the tissue was directly fixed in paraformaldehyde (PFA) 4% in phosphate-buffered saline (PBS) pH 7.4 for histological evaluation. The remaining tissue was cryopreserved in 50% RPMI medium, 40% FCS, and 10% DMSO. On the day of engraftment, the recently resected tumor tissue was grafted onto a well-vascularized part of the CAM (Figure 1). The tissue samples were cultivated for 7 days, and daily photo documentation was performed using a Leica M205A microscope. After the experimental period, the tissue including the surrounding CAM was cut out and the eggs were immediately discarded in liquid nitrogen. The samples were fixed in paraformaldehyde (PFA) 4% in PBS pH 7.4 for 24 h, followed by 6 days in 0.02% sodium azide before embedding and staining.
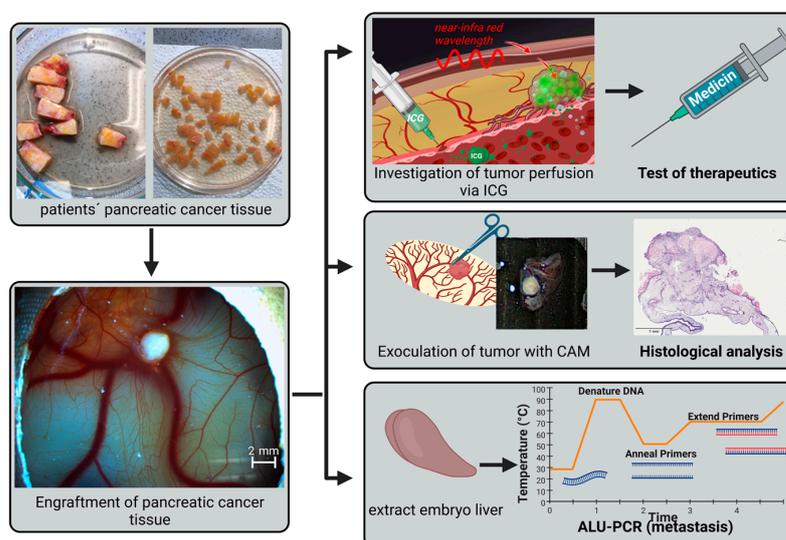

Figure 1. Schematic workflow: Patient-derived pancreatic cancer tissue is cut into smaller fragments and subsequently engrafted onto the CAM. While the tissue is kept vital by the CAM, intravenously injected ICG can be used to visualize perfusion in the human graft and, thus, various therapeutics can be tested intravenously. After the tissue has been removed from the CAM, histological analysis of the tissue as well as the examination for metastases using ALU-PCR can be performed (created with BioRender.com).

2.3. Cryopreservation of Tumor Tissue

Parts of the patient-derived tumor tissue were cryopreserved. Hence, thin slices of patient tumor tissue were cut into approximately 3 mm × 3 mm × 1 mm pieces and then placed in a cryovial with a freezing medium, consisting of 50% RPMI medium, 40% FCS, and 10% DMSO. The vials were then inserted in a Mr. Frosty™ Freezing Container (Waltham, MA, USA) for 24 h at −80 °C and then placed in cryoboxes for long-term storage. After at least 7 days, the tissue was then defrosted by placing the cryovial in a water bath at 37 °C for 2 min, washed twice with fresh RPMI media, and after 1 h of reactivation in RPMI medium, the tissue was engrafted onto the CAM as described in Section 2.2.

2.4. Intravenous Indocyanine Injection

ICG was injected intravenously to monitor the intratumoral perfusion. ICG was diluted to 50 μM with 0.9% sodium chloride to obtain a final concentration of 0.3 mg/kg. The fluorescence maximum in blood is at 830 nm [45]. The procedure was recorded using the Medtronics Elevision IR (VSIII) fluorescence system (Medtronic®, Meerbusch, Germany) near-infrared video-measuring device. The injection was performed using a 1 mL syringe (Norm-Ject HENKE, Tuttlingen, Germany) with a 33 G needle (Hypodermic Needles, 33 G 0.20 mm × 4 mm, MESORAM, Putzbrunn, Germany). The syringe was vented, and 50 μL of the ICG solution was injected intravenously into the chicks' bloodstream (Figure 2). A video of the IR signal and visible light was recorded during the injection process (Figure 2) for 15 min after the needle was removed, and bleeding was stopped with a sterile compress (5 cm × 5 cm, ES Compresses, HARTMANN, Heidenheim, Germany) (Supplementary Videos S1–S4). Afterwards, the signal intensity was analyzed using Image J (v1.54, 1.8.0_345) and the implemented measurement tool to measure the ICG signal brightness from the tumor and the surrounding CAM according to their RBG value.
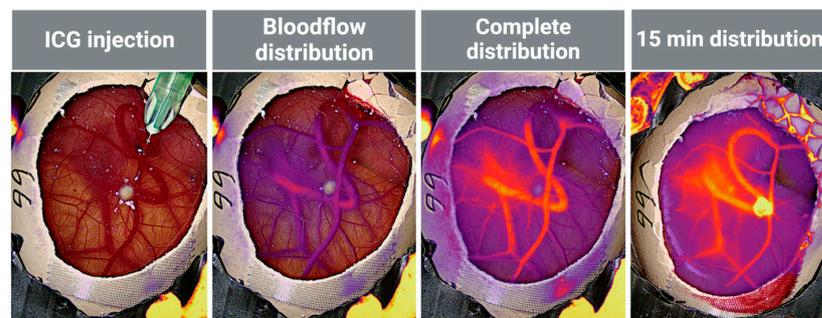

Figure 2. Schematic overview of ICG injection into the CAM vessels. ICG was injected intravenously into the amniotic blood system. Within seconds, the contrast agent was distributed throughout the vasculature, allowing detection by near-infrared measurement. After 15 min, the dye was detected in the tumor tissue (created with BioRender.com).

2.5. Histology and Immunohistochemistry

The fixed tumors were placed in an Automatic Tissue Processor (TP10120, Leica, Nussloch, Germany) for dehydration with increasing alcohol concentrations and xylene. Afterward, each tumor was embedded in a paraffin embedding station EG1150 H from LEICA. The paraffin blocks were sectioned, deparaffinized in xylene, hydrated in a descending alcohol series, and then stained with hematoxylin solution Gill N°.3 (Sigma-Aldrich, Taufkirchen, Germany) and eosin Y 0.1% (H&E). Furthermore, immunohistological stainings were performed by using antibodies against Cytokeratin-7 (clone: OV TL12/30, host: mouse, DAKO, Santa Clara, CA, USA) and KI-67 (clone: MIB-1, host: mouse, Abcam, Cambridge, UK) in a fully automated manner according to the manufacturer's standard protocol (Figure 3). Histological sections (5×, 10×, 20×, 40×, and 60×) were digitized using a microscopy slide scanner for virtual microscopy (Fritz, Precipoint, Garching bei München, Germany).

2.6. Polymerase Chain Reaction (PCR)

First, the tumor was removed from the CAM by using scissors; shortly after, the chick's liver was dissected by using tweezers and single-use scalpels. The preparation kit was cleaned using ethanol and flamed for sterilization for the next dissection. Then, the specimens were placed in liquid nitrogen in a 2 mL Eppendorf tube and 800 μL of extraction solution (50 mM Tris-HCL, pH8.0; 25 mM EDTA and 400 mM NaCl), 100 μL 10% SDS, and 20 μL proteinase K (10 mg/mL) were added. The extract was homogenized and incubated at 65 °C for 3 h. After homogenization at 50 °C, the dilute was centrifuged at 12,600 rpm for 15 min. The supernatant was tossed away, and the pellet was resuspended in 100%

isopropanol, followed by another centrifugation step at 12,600 rpm for 5 min. Finally, the pellet was resuspended in 70% EtOH and washed twice, before resuspension in ddH$_2$O to dissolve the DNA pellet. The DNA samples were then stored at 4 °C. The extracted genomic DNA (gDNA) was subject of an ALU-PCR. A 247 bp amplicon was amplified using a primer set used in several previous studies [43,46]: forward 5′-GTGGCTCACGCCTGTAATC-3′; reverse 5′-CAGGCTGGAGTGCAGTGG-3′. The reaction mixture for the ALU-PCR consisted of 0.2 μM of each primer, 1 U Thermo Polymerase, 0.5 μL dNTPs, and 0.5 μL DNA and 1× Thermol pol Buffer. ddH$_2$O was added to a total reaction volume of 25 μL. To amplify the ALU repeat in a thermocycler (Bio Rad C100 Touch, Feldkirchen, Germany), the polymerase was heat activated at 95 °C for 3 min, followed by 35 cycles of 30 s denaturation at 95°C, 30 s annealing at 62 °C, and 45 s elongation at 72 °C. After that, the sample was kept at 72 °C for 5 min and then stored at 4 °C for further use. The negative control contained 0.5 μL ddH$_2$O instead of DNA. For the positive control, the gDNA of human renal cystic tissue and human pancreatic cancer tissue was used. The PCR products were visualized by Rotistain (Thermo Fisher Waltham, MA USA) on a 1% agarose gel in 1× Tris acetate EDTA (TAE).
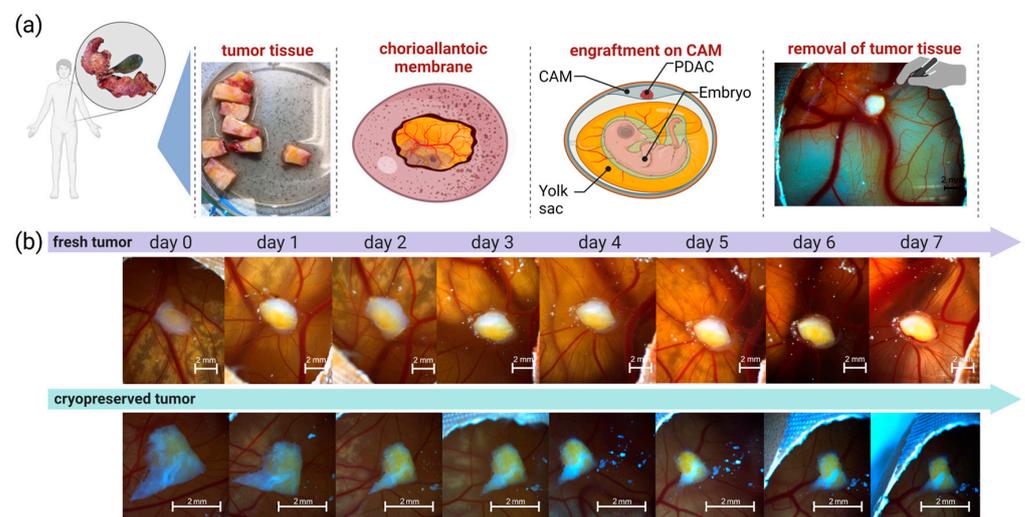

Figure 3. (**a**) Timelapse of recently resected and cryopreserved pancreatic cancer tissue engrafted onto the CAM. Schematic overview of the workflow. (**b**) Microscopic photo documentation over the experimental period (created with BioRender.com).

3. Results

3.1. Engraftment of Pancreatic Tumor Tissue on the CAM

Patient-derived xenografts (PDX) from recently resected and cryopreserved pancreatic cancer tissue were studied in the CAM model. The recently resected tumor tissue was applied to the CAM on the day of surgery (Figure 3), while the cryopreserved tumor tissue was stored at −80 °C for at least 7 days. Figure 3 displays two representative CAM models with recently resected and cryopreserved tumors over the experimental period of 7 days (Figure 3). Macroscopical analysis of the PDX demonstrates no discernable dissimilarities in tumor growth patterns.

Histological analysis of the cryopreserved PDX resulted in retained neoplastic tissue with intact structure (i.e., comprised of stromal, vascular, and epithelial tissue) in line with the untreated primary tumor (Figures 4a and 5a). The tumor was partly distinguishable from the surrounding stroma and the CAM and tumor cells were detected inside the CAM (Figures 4b and 5b). Part of the cryopreserved tissue remained vital, as confirmed by intensely stained, enlarged nuclei and preserved atypical ducts. In contrast, part of the tissue presents the classic signs of necrosis: karyorrhexis, cellular debris, infiltrating granulocytes, and calcification typical of older necrotic tissue (Figure 5b). H&E, Cytokeratin7, and Ki-67

staining revealed solid or dispersed growth of ductal pancreatic adenocarcinoma presenting large, strikingly polymorphous tumor cells surrounding empty lumina of varying size (Figures 4b and 5b). Furthermore, pancreatic tumor tissue indicated the presence of periductal fibrosis. The lobular parenchyma was partially replaced by desmoplastic stroma with irregular pancreatic ducts, and the cells demonstrated marked nuclear enlargement and pleomorphism (Figures 4 and 5).
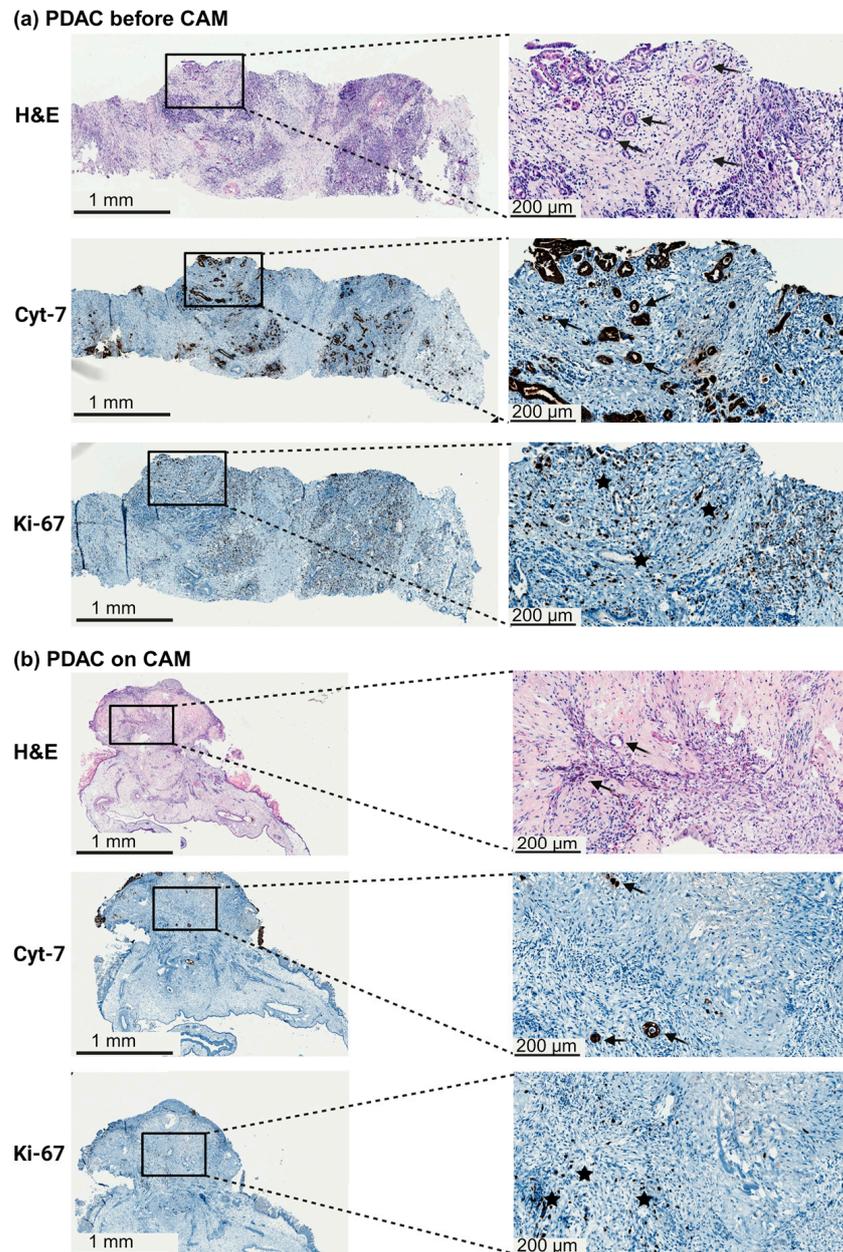

Figure 4. Histological examination of a PDX before and after growth on the CAM. Whole slide H&E, Cytokeratin7, and Ki-67 staining. (**a**) Recently resected PDAC tissue on the day of surgical resection before engraftment on the CAM. (**b**) Recently resected PDAC after 7 days of engraftment on the CAM. Scale bar = 1 mm and 200 μm, 100× magnification (created with BioRender.com). Atypical ducts of the PDAC (arrows), elevated proliferation within the tumor visible by increased nuclear Ki-67 staining (stars).
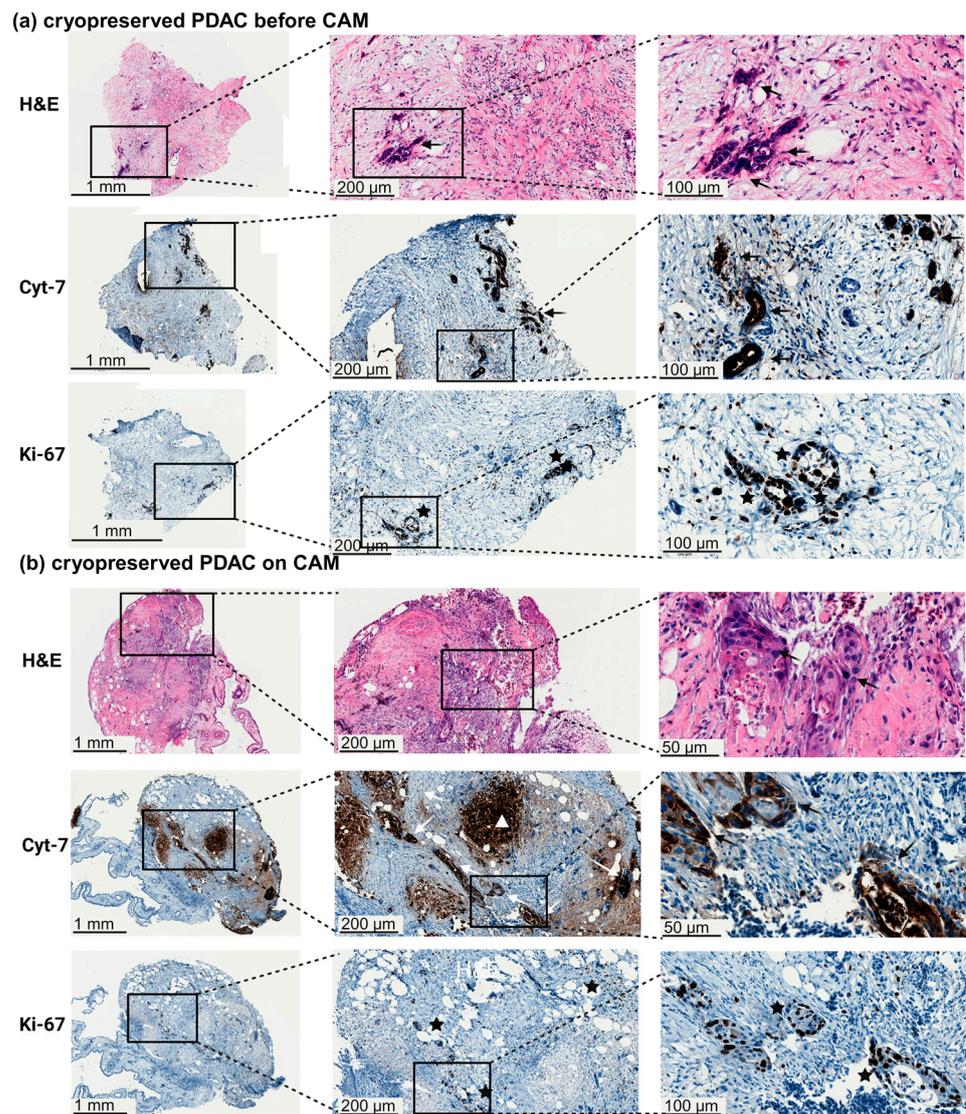
(a) cryopreserved PDAC before CAM

(b) cryopreserved PDAC on CAM

Figure 5. Histological examination of a PDX before and after growth on the CAM. Whole slide H&E, Cytokeratin7, and Ki-67 staining. (**a**) Cryopreserved PDAC tissue on the day of surgical resection before engraftment onto the CAM (**b**) Cryopreserved PDAC after 7 days of engraftment on the CAM. Scale bar = 1 mm, 200 µm, 100 µm and 50 µm, 100× magnification (created with BioRender.com). Atypical ducts of the PDAC (arrows), elevated proliferation within the tumor visible by increased nuclear Ki-67 staining (stars), classic signs of necrosis (triangle).

3.2. Visualization of Tumor Perfusion by Intravenous ICG Injection

This study aimed at visualizing intratumoral perfusion using ICG and near-infrared imaging. Directly after the injection, the ICG was detected in the larger blood vessels shown in Figure 6a. To investigate the change in signal intensity over time, a solution of embryonic blood and ICG (40 µM with 0.9% sodium) was applied as a reference point for quantification. After 15 min, ICG accumulated in the tumor tissue, resulting in the detection of a strong fluorescence signal (Figure 6b). This confirms that the tumor tissue is connected to the embryonic circulation of the embryo. Furthermore, we investigated the accumulation by comparing the signal intensity using ImageJ (Figure 6c,d). Figure 6d summarized the signal intensities measured for each CAM and each of three patients according to their RBG brightness. In total, engrafted tumor material was compared and resulted in a significantly enriched signal inside the tumor for patient X and Y (Figure 6d, Supplementary Figure S1). Figure 6e presents an outline of the signal intensity for four engrafted tumors of patient X,

removed including surrounding CAM. The fluorescent dye could be identified in three of the four tissue samples, whereby only a weak signal was detectable in one sample. These results provide the basis for testing intravenously injected therapeutics in future projects and evaluating their effect on tumor growth or metastasis.
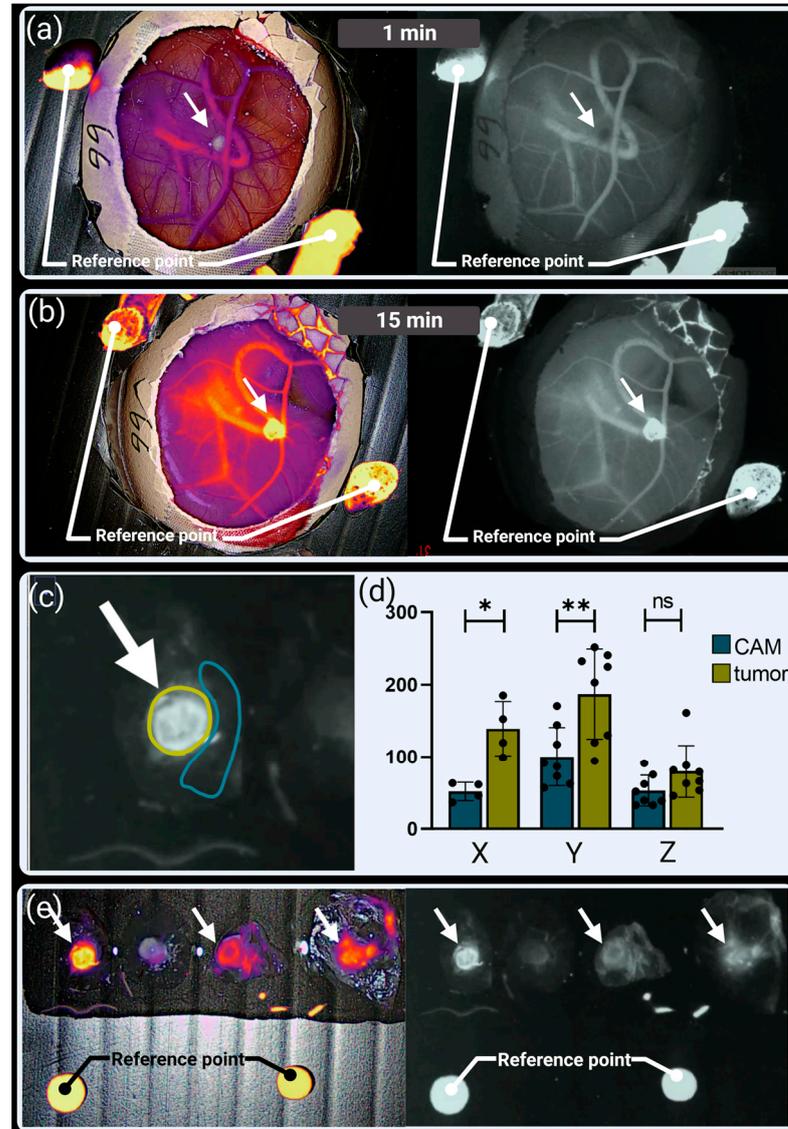

Figure 6. Near-infrared measurements after intravenous injection of ICG. (**a**,**b**) the arrows indicates the position of the engrafted tumor, (**c**,**e**) the arrow indicates a clearly perfused tumor. (**a**) IR video and fused overlay video of the CAM 1 min after injection (Supplementary Videos S1 and S2). (**b**) IR video and fused overlay video of the CAM model 15 min after injection (Supplementary Videos S3 and S4). (**c**) Photo of ICG signal intensity of the accumulated ICG in the tumor. The Image J implemented section tool was used with the measurement tool to measure the ICG signal brightness from the tumor and the surrounding CAM according to their RBG value. (**d**) ICG signal intensity comparing CAM and tumor of three different patients (pat. X, Y, Z). ICG brightness of the extracted tumor with surrounding CAM. ICG signal intensity, 15 min after ICG injection. Brightness is indicated from 0 [black] to 255 [white] according to RGB values. The CAM measurements are displayed in cyan and the tumor measurements in green color. Data was analyzed by one-way ANOVA, followed by a Tukey's test (** < 0.01, * < 0.05, ns = non-significant)). (**e**) IR video and fused overlay video of the removed tumor with the surrounding CAM of four representative tumors of patient X with reference points (created with BioRender.com).

3.3. Detection of Metastasis Using Alu PCR

To determine whether metastases of the primary tumor tissue occurred in the organs of the embryo, an Alu PCR of the chick´s liver was performed at the end of the experimental period. For the detection of human cancer cells, human-specific Alu repeat sequences were used. Gel electrophoresis of the PCR products of PDAC tissue samples from three different patients, as well as human polycystic kidney tissue, showed the expected signal at 247 bp (Figure 7, lanes 11, 13, 14). Moreover, human Alu repeats were analyzed in the embryo´s liver of CAM models bearing tissue of three PDAC patients. Here, DNA of human tumor cells (Figure 7, lanes 1–8) was detected, indicating that the primary tumor tissue had released cells into the bloodstream, which had spread into the organism. In contrast, no Alu signal was present in the livers of CAM models bearing no tumor (Figure 7, lanes 9, 10).
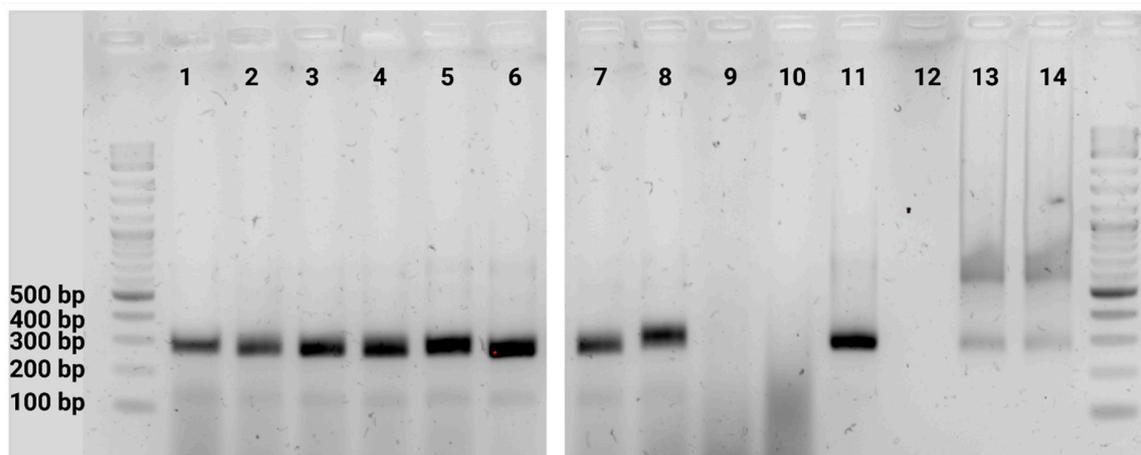

Figure 7. Alu sequence 247 PCR. Embryo's liver of CAM model engrafted with pancreatic tumor tissue of patient X (1–4), patient Y (5–6), patient Z (7–8). Embryo's liver of CAM model bearing no tumor (9–10). Human renal cystic tissue (11), water control (12), and human pancreatic cancer tissue (13–14). Gel electrophoresis of the PCR products derived from the pancreas and kidney serve as positive controls (11, 13, 14). The DNA template used in each lane is shown at the top. The product size was as expected at a height of 257 bp for pancreatic cancer tissue as well as kidney tissue (created with BioRender.com).

4. Discussion

4.1. Intratumoral Perfusion of Pancreatic Cancer Tissue Cultivated on CAM and Future Implications

Anastomoses between the pancreatic cancer vessel and the CAM vessel were detected using near-infrared imaging, showing how the grafted tumor tissue is thus supplied with nutrients, growth factors, and stem cells of the developing embryo. This finding lays the foundation for the application and evaluation of intravenously administered therapeutics for the treatment of PDAC in the CAM model. Potentially applied substances reach the target site through the bloodstream and the effects can be analyzed using a clinically relevant form of application of chemotherapeutic agents. The usage of ICG angiography is a simple, fast, and cost-effective method applied to the CAM model to verify intratumoral perfusion before applying intravenous therapies. Moreover, side effects of ICG application are very rare [47–50].

Furthermore, the anastomoses between the CAM and the tumor vessel enable the formation of metastases. Originating from the primary tissue, tumor cells enter the bloodstream via microvessels and attach to secondary sites. By Alu PCR, human DNA in the liver of the embryo was detected, which indicates the development of metastases shed from the primary site. These results (Figure 7) show a high level of intertumoral heterogeneity between the patients, highlighting the need for future studies towards personalized medicine.

The Alu-PCR of chicken organs could become a standardized method for studying the process of metastases which is the main cause of death in pancreatic cancer patients in the future. Histological analysis was performed for all the dissected chick livers and, so far, no metastases have been detected during the histological examination. Our hypothesis is that individual metastatic cells are yet too small and cannot be detected histologically; however, exogenous human DNA can be detected using ALU PCR. Moreover, dormancy often follows the extravasation of cells at the secondary site, thus it can take some time before these cancers start proliferating in the metastatic target organ [51]. Additionally, this approach could be enhanced by pancreatic cancer-specific primers against mRNA CA 19-9, CA 125, miRNA21, and M2-PK and primers to test genetic mutations such as KRAS [52,53]. These tests can be conducted by utilizing digital droplet PCR (ddPCR) to examine the impact of the recommended drugs of the molecular tumor board on the tumor and its metastatic behavior. However, there are still some limitations in studying metastasis using the CAM model, especially regarding the short time frame available to conduct experiments. Therefore, the majority of cancer cells are not able to produce macroscopically visible colonies in secondary organs within 7 days, and cancer cells would not have had enough time to generate microscopical metastases [54]. After seven days, tumors that had grown on the CAM can be divided into two parts, whereby one tissue part is transplanted onto a new CAM while the other tissue part could be used for further experiments [55]. We have shown that this procedure can be repeated five to seven times for three different sections of the osteosarcoma from one patient.

In ongoing studies, the aggressiveness of individual PDAC samples grown on the CAM and their capacity for early metastasis with the long-term oncologic outcome and metastatic spread could be correlated for each patient. Regarding current studies and clinical trials evaluating neoadjuvant therapy concepts for PDAC patients, the CAM model could be a highly interesting diagnostic tool to identify patients in need of such a therapy.

4.2. Characterization and Optimization Employing the Molecular Communications Paradigm

It is of utmost importance to understand the distribution of drug molecules and drug carriers, such as nanoparticles inside the circulatory system, and their ability to reach target sites to design and optimize drug delivery systems. Molecular communications (MC) is a novel, nature-inspired communications paradigm where the information is encoded in the properties of molecules [56] instead of electromagnetic waves (Figure 8). In the past years, the MC paradigm has been exploited to gain more insight into and the control of the operation of biological systems and to design and implement synthetic MC systems. For example, in medical applications, MC systems are expected to facilitate the distribution of nano-scale sensor networks for the detection of diseased cells and allow the control of actuators for targeted drug release [57].
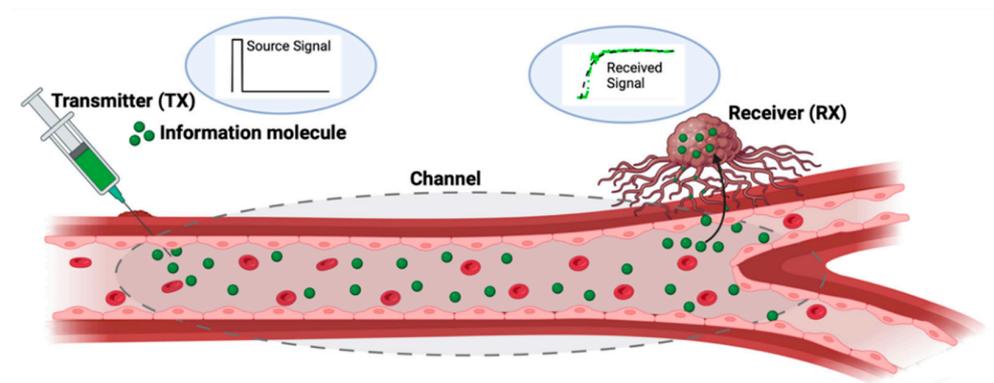

Figure 8. Molecular communication system model for injecting ICG into the model and the accumulation in the tumor. In this framework, the injection is interpreted as the transmitter (TX) of information-carrying molecules (here: ICG molecules), the tumor as the receiver (RX) of information, and the CAM model as the channel where the ICG is propagating (created with BioRender.com).

Especially for targeted drug delivery systems, MC is a suitable framework for design, analysis, and optimization. Based on the MC paradigm, the drug release (e.g., from a nanoparticle or by injection), the diseased cell, and the drug propagation environment are regarded as transmitter, receiver, and random channel, respectively [35,58]. This interpretation allows for the comparison of drug delivery systems to conventional communication systems, providing a multitude of tools for the theoretical analysis and optimization of such systems. In many practical drug delivery scenarios, the concentration of drug molecules is supposed to remain within a therapeutic range over a prolonged period [59]. To design a drug delivery system, for example, a so-called end-to-end MC system model (end-to-end means a simulation model capturing all dynamics from injection to reception) can be used to relate the number of drug molecules in a target region to the design of the drug release dynamics (Figure 8) [60]. This allows for the further optimization of the drug delivery system without the need for a large amount of wet lab experiments. Regarding the scenario considered in this study, the injection, propagation, and accumulation of ICG in the tumor can be interpreted as a molecular communication system. As shown in Figure 8, the injection of ICG into the vessels resembles the transmitter, the ICG molecules are the carriers that propagate in the circulatory system, and the tumor is the receiver of information. In future works, the MC paradigm could be implemented to obtain powerful communication–theoretical models to relate the transmit signal, i.e., the amount and duration of ICG injection, to the received signal, i.e., the gradual increase in ICG in the tumor. These models provide further insight into the distribution of ICG inside the CAM model and facilitate the optimization of the system, to determine the optimal amount of injected ICG and preferable injection times. Moreover, as the distribution of ICG can reveal an indication of the distribution of drug molecules inside the model, the obtained simulation models can later be used to study the distribution and targeting of drug molecules.

4.3. Organoids and CAM Model

As already shown by many research groups, the CAM not only offers the possibility of cultivating cell lines, tumor tissue, and spheres but also the growth of organoids. The combination of these two methods was initially used for research in the field of angiogenesis, but, in the meantime, organoids of various organs and tissues have been studied in this model. Varzideh et al. engrafted three-dimensional cardiac organoids containing human ESCs-derived progenitor cells, endothelial cells, as well as mesenchymal stem cells onto the CAM, whereupon they induced a strong angiogenic response [61]. Wörsdörfer et al. demonstrated the functional connection of organoids obtained by co-culturing human mesodermal progenitors with progenitor cell types to the host blood circulation [42]. A connection to the chick´s circulating system was also observed by Schmidt et al. while cultivating blood vessel organoids in the CAM model [62]. The recovery of tubulogenic capacity was shown by Kaisto et al., as kidney spheroids were grafted onto the CAM [63]. In future projects, organoids obtained from pancreatic cancer could be cultured on the CAM to test chemotherapeutic regimens.

Meanwhile, the CAM model could also be used as a complementary in vitro technique to study perfusion. Microfluidic human organoids-on-chip mimic the tumor microenvironment with its multicellular architecture, chemical gradient, mechanical pressure, and vascularization. Therefore, they allow the control of minimal microenvironmental components important for tumor growth and invasion, in a way that is not possible in the CAM model. So, while the CAM model allows for the creation of a physiological environment, especially good for drug testing, the organoids-on-chips could be used to systematically control and study singular components involved in tumor perfusion [64,65].

4.4. Impact of Cryopreservation on Personalized Therapy Approaches Recommended by the Molecular Tumor Board

A molecular tumor board is a forum in which doctors from different disciplines, including oncology, radiology, surgery, pathology, molecular biology, and computer science,

discuss the multidisciplinary treatment of tumor patients. The difference between the conventional tumor board and the molecular tumor board is the presence of geneticists, scientists, and bioinformaticians, as greater importance is attributed to the molecular profile of the patient's tumor tissue [27]. While patients need four to six weeks for convalescence after surgery to receive adjuvant treatment, this period offers the opportunity to test suitable chemotherapeutics. The tumor board consultation usually occurs within 3 weeks after surgery. Thus, the use of cryopreserved tissue in the CAM model provides the possibility to test and evaluate the proposed therapeutic approaches before the patient begins treatment. This innovative approach is projected to not only enhance treatment effectiveness but also minimize side effects, mitigate toxicity, limit drug wastage, and cut healthcare costs in contrast with traditional treatment methods. By testing therapeutics in the CAM model, the type of drug, composition, and injection strategy can be optimized by evaluating reproducible experiments. Therefore, the MC paradigm can help to build simulation models to analyze drug accumulation in the tumors and develop algorithms to optimize injection strategies for increasing the accumulation at the target site while reducing side effects in other regions.

The potential aim for the future is the integration of drug testing in the CAM model into the general as well as the molecular tumor board in our clinic. As a first step, already known molecular tumorboard therapeutic suggestions of past patients will be tested on their cryopreserved tumor samples on the CAM. This approach could provide patients who have already received a result from the molecular tumor board with the opportunity to test the most promising therapy in this model and compare it with the standard therapy. In addition, this could be advantageous as the evaluation of the molecular tumor board can change due to mutations in the tumor. Therefore, even if mutations occur, the use of cryopreserved tissue can enable a more precise approach to personalized therapy. Thus, this new approach could facilitate informed decision making regarding personalized treatment of patients suffering from PDAC.

4.5. Advantages of the CAM Model as a Drug-Testing Platform

The CAM model has the potential to be used as a platform for personalized medicine. If specimens from tumor biopsies can be efficiently grafted onto the CAM, this could lead to new insights into the characteristics of individual tumor samples and might offer a platform for individual drug testing. Since the mouse model is a mammal, it is physiologically more similar to the human species than the avian CAM model; however, the CAM model presents many advantages for testing therapeutics. As the embryo's immune system is not fully developed, rejection of the human graft is avoided, and administered substances are metabolized less quickly. Unlike animal models, immunodeficient bred strains are not required. The tissue can be monitored more conveniently and regularly during the experiment through the window in the eggshell, allowing the effects of therapeutics to be recorded in greater detail with the offset of less molecular information. As the methods and models used for testing drugs for personalized treatment should present a short time frame since there is a maximum of 6 weeks available between surgery and the start of the treatment, the CAM model enables the testing of potential drugs within one week. Whole genome sequencing of patients' tumor tissue remains the gold standard for detecting significant mutations, epigenetic upregulations, and molecular target sites. Unfortunately, whole genome sequencing, especially single-cell sequencing, is highly time consuming and expensive. The simplicity, low cost, and high reproducibility strengthen the use of this model as an innovative drug-testing platform. While the CAM model can be a useful tool to gain a more profound understanding of the complex nature and heterogeneity of PDAC, it may bridge the gap between cell-based and animal-based assays [66].

5. Conclusions

The CAM model provides an optimal alternative to previous animal models in cancer research. Using ICG angiography, we were able to confirm that human pancreatic tumor

tissue is connected to the circulating system of the embryo, thereby enabling the testing of intravenously administered therapeutics. Furthermore, using Alu PCR, we were able to detect human cells in the organs of the embryo indicating metastasis. Finally, we have shown that cryopreserved tissue can be preserved by the CAM, which marks a major step towards personalized therapy on the recommendation of the tumor board.

References

1. Schima, W.; Ba-Ssalamah, A.; Kölblinger, C.; Kulinna-Cosentini, C.; Puespoek, A.; Götzinger, P. Pancreatic adenocarcinoma. *Eur. Radiol.* **2007**, *17*, 638–649. [CrossRef] [PubMed]
2. Sung, H.; Ferlay, J.; Siegel, R.L.; Laversanne, M.; Soerjomataram, I.; Jemal, A.; Bray, F. Global Cancer Statistics 2020: GLOBOCAN Estimates of Incidence and Mortality Worldwide for 36 Cancers in 185 Countries. *CA Cancer J. Clin.* **2021**, *71*, 209–249. [CrossRef] [PubMed]
3. Shield, K.D.; Ferlay, J.; Jemal, A.; Sankaranarayanan, R.; Chaturvedi, A.K.; Bray, F.; Soerjomataram, I. The global incidence of lip, oral cavity, and pharyngeal cancers by subsite in 2012. *CA Cancer J. Clin.* **2017**, *67*, 51–64. [CrossRef] [PubMed]
4. Rahib, L.; Smith, B.D.; Aizenberg, R.; Rosenzweig, A.B.; Fleshman, J.M.; Matrisian, L.M. Projecting cancer incidence and deaths to 2030: The unexpected burden of thyroid, liver, and pancreas cancers in the United States. *Cancer Res.* **2014**, *74*, 2913–2921. [CrossRef]
5. Ferlay, J.; Colombet, M.; Soerjomataram, I.; Mathers, C.; Parkin, D.M.; Piñeros, M.; Znaor, A.; Bray, F. Estimating the global cancer incidence and mortality in 2018: GLOBOCAN sources and methods. *Int. J. Cancer* **2019**, *144*, 1941–1953. [CrossRef] [PubMed]
6. Ferlay, J.; Colombet, M.; Soerjomataram, I.; Dyba, T.; Randi, G.; Bettio, M.; Gavin, A.; Visser, O.; Bray, F. Cancer incidence and mortality patterns in Europe: Estimates for 40 countries and 25 major cancers in 2018. *Eur. J. Cancer* **2018**, *103*, 356–387. [CrossRef]
7. Hu, J.-X.; Zhao, C.-F.; Chen, W.-B.; Liu, Q.-C.; Li, Q.-W.; Lin, Y.-Y.; Gao, F. Pancreatic cancer: A review of epidemiology, trend, and risk factors. *World J. Gastroenterol.* **2021**, *27*, 4298–4321. [CrossRef]
8. Bardeesy, N.; DePinho, R.A. Pancreatic cancer biology and genetics. *Nat. Rev. Cancer* **2002**, *2*, 897–909. [CrossRef]
9. Chuong, M.D.; Herrera, R.; Ucar, A.; Aparo, S.; De Zarraga, F.; Asbun, H.; Jimenez, R.; Asbun, D.; Narayanan, G.; Joseph, S.; et al. Causes of Death Among Patients with Initially Inoperable Pancreas Cancer After Induction Chemotherapy and Ablative 5-fraction Stereotactic Magnetic Resonance Image Guided Adaptive Radiation Therapy. *Adv. Radiat. Oncol.* **2023**, *8*, 101084. [CrossRef]
10. Pantel, K.; Alix-Panabières, C. Bone marrow as a reservoir for disseminated tumor cells: A special source for liquid biopsy in cancer patients. *Bonekey Rep.* **2014**, *3*, 584. [CrossRef]

11. Effenberger, K.E.; Schroeder, C.; Hanssen, A.; Wolter, S.; Eulenburg, C.; Tachezy, M.; Gebauer, F.; Izbicki, J.R.; Pantel, K.; Bockhorn, M. Improved Risk Stratification by Circulating Tumor Cell Counts in Pancreatic Cancer. *Clin. Cancer Res.* **2018**, *24*, 2844–2850. [CrossRef]

12. Vanharanta, S.; Massagué, J. Origins of metastatic traits. *Cancer Cell* **2013**, *24*, 410–421. [CrossRef]

13. Agudo, J.; Aguirre-Ghiso, J.A.; Bhatia, M.; Chodosh, L.A.; Correia, A.L.; Klein, C.A. Targeting cancer cell dormancy. *Nat. Rev. Cancer* **2023**. [CrossRef]

14. Kolbeinsson, H.M.; Chandana, S.; Wright, G.P.; Chung, M. Pancreatic Cancer: A Review of Current Treatment and Novel Therapies. *J. Investig. Surg.* **2023**, *36*, 2129884. [CrossRef]

15. Jentzsch, V.; Davis, J.A.A.; Djamgoz, M.B.A. Pancreatic Cancer (PDAC): Introduction of Evidence-Based Complementary Measures into Integrative Clinical Management. *Cancers* **2020**, *12*, 3096. [CrossRef]

16. Jiang, S.; Fagman, J.B.; Ma, Y.; Liu, J.; Vihav, C.; Engstrom, C.; Liu, B.; Chen, C. A comprehensive review of pancreatic cancer and its therapeutic challenges. *Aging* **2022**, *14*, 7635–7649. [CrossRef]

17. Zeng, S.; Pöttler, M.; Lan, B.; Grützmann, R.; Pilarsky, C.; Yang, H. Chemoresistance in Pancreatic Cancer. *Int. J. Mol. Sci.* **2019**, *20*, 4504. [CrossRef]

18. Lokman, N.A.; Elder, A.S.F.; Ricciardelli, C.; Oehler, M.K. Chick chorioallantoic membrane (CAM) assay as an in vivo model to study the effect of newly identified molecules on ovarian cancer invasion and metastasis. *Int. J. Mol. Sci.* **2012**, *13*, 9959–9970. [CrossRef]

19. Sommers, S.C.; Sullivan, B.A.; Warren, S. Heterotransplantation of human cancer. III. Chorioallantoic membranes of embryonated eggs. *Cancer Res.* **1952**, *12*, 915–917. [PubMed]

20. Kunzi-Rapp, K.; Genze, F.; Küfer, R.; Reich, E.; Hautmann, R.E.; Gschwend, J.E. Chorioallantoic membrane assay: Vascularized 3-dimensional cell culture system for human prostate cancer cells as an animal substitute model. *J. Urol.* **2001**, *166*, 1502–1507. [CrossRef] [PubMed]

21. Mapanao, A.K.; Che, P.P.; Sarogni, P.; Sminia, P.; Giovannetti, E.; Voliani, V. Tumor grafted—Chick chorioallantoic membrane as an alternative model for biological cancer research and conventional/nanomaterial-based theranostics evaluation. *Expert Opin. Drug Metab. Toxicol.* **2021**, *17*, 947–968. [CrossRef]

22. Ribatti, D. The chick embryo chorioallantoic membrane (CAM). A multifaceted experimental model. *Mech. Dev.* **2016**, *141*, 70–77. [CrossRef]

23. DeBord, L.C.; Pathak, R.R.; Villaneuva, M.; Liu, H.-C.; Harrington, D.A.; Yu, W.; Lewis, M.T.; Sikora, A.G. The chick chorioallantoic membrane (CAM) as a versatile patient-derived xenograft (PDX) platform for precision medicine and preclinical research. *Am. J. Cancer Res.* **2018**, *8*, 1642–1660.

24. Ribatti, D. The chick embryo chorioallantoic membrane patient-derived xenograft (PDX) model. *Pathol. Res. Pract.* **2023**, *243*, 154367. [CrossRef]

25. Majumder, S.; Chari, S.T.; Ahlquist, D.A. Molecular detection of pancreatic neoplasia: Current status and future promise. *World J. Gastroenterol.* **2015**, *21*, 11387–11395. [CrossRef]

26. Zhen, D.B.; Safyan, R.A.; Konick, E.Q.; Nguyen, R.; Prichard, C.C.; Chiorean, E.G. The role of molecular testing in pancreatic cancer. *Therap. Adv. Gastroenterol.* **2023**, *16*, 17562848231171456. [CrossRef]

27. Behel, V.; Noronha, V.; Choughule, A.; Shetty, O.; Chandrani, P.; Kapoor, A.; Bondili, S.K.; Bajpai, J.; Kumar, R.; Pai, T.; et al. Impact of Molecular Tumor Board on the Clinical Management of Patients with Cancer. *JCO Glob. Oncol.* **2022**, *8*, e2200030. [CrossRef]

28. Idrisova, K.F.; Simon, H.-U.; Gomzikova, M.O. Role of Patient-Derived Models of Cancer in Translational Oncology. *Cancers* **2022**, *15*, 139. [CrossRef]

29. Nakaseko, Y.; Ishizawa, T.; Saiura, A. Fluorescence-guided surgery for liver tumors. *J. Surg. Oncol.* **2018**, *118*, 324–331. [CrossRef]

30. Soltesz, E.G.; Kim, S.; Kim, S.-W.; Laurence, R.G.; De Grand, A.M.; Parungo, C.P.; Cohn, L.H.; Bawendi, M.G.; Frangioni, J.V. Sentinel lymph node mapping of the gastrointestinal tract by using invisible light. *Ann. Surg. Oncol.* **2006**, *13*, 386–396. [CrossRef]

31. Weixler, B.; Lobbes, L.A.; Scheiner, L.; Lauscher, J.C.; Staubli, S.M.; Zuber, M.; Raptis, D.A. The Value of Indocyanine Green Image-Guided Surgery in Patients with Primary Liver Tumors and Liver Metastases. *Life* **2023**, *13*, 1290. [CrossRef]

32. Chauhan, N.; Cabrera, M.; Chowdhury, P.; Nagesh, P.K.B.; Dhasmana, A.; Pranav; Jaggi, M.; Chauhan, S.C.; Yallapu, M.M. Indocyanine Green-based Glow Nanoparticles Probe for Cancer Imaging. *Nanotheranostics* **2023**, *7*, 353–367. [CrossRef]

33. Kue, C.S.; Tan, K.Y.; Lam, M.L.; Lee, H.B. Chick embryo chorioallantoic membrane (CAM): An alternative predictive model in acute toxicological studies for anti-cancer drugs. *Exp. Anim.* **2015**, *64*, 129–138. [CrossRef]

34. Vargas, A.; Zeisser-Labouèbe, M.; Lange, N.; Gurny, R.; Delie, F. The chick embryo and its chorioallantoic membrane (CAM) for the in vivo evaluation of drug delivery systems. *Adv. Drug Deliv. Rev.* **2007**, *59*, 1162–1176. [CrossRef]

35. Chude-Okonkwo, U.A.K.; Malekian, R.; Maharaj, B.T.; Vasilakos, A.V. Molecular Communication and Nanonetwork for Targeted Drug Delivery: A Survey. *IEEE Commun. Surv. Tutor.* **2017**, *19*, 3046–3096. [CrossRef]

36. Torchilin, V.P.; Lukyanov, A.N. Peptide and protein drug delivery to and into tumors: Challenges and solutions. *Drug Discov. Today* **2003**, *8*, 259–266. [CrossRef]

37. Salehi, S.; Moayedian, N.S.; Haghjooy Javanmard, S.; Alarcon, E. Lifetime Improvement of a Multiple Transmitter Local Drug Delivery System Based on Diffusive Molecular Communication. *IEEE Trans. Nanobiosci.* **2018**, *17*, 352–360. [CrossRef]

38. Femminella, M.; Reali, G.; Vasilakos, A.V. A Molecular Communications Model for Drug Delivery. *IEEE Trans. Nanobiosci.* **2015**, *14*, 935–945. [CrossRef]

39. Chahibi, Y.; Pierobon, M.; Song, S.O.; Akyildiz, I.F. A Molecular Communication System Model for Particulate Drug Delivery Systems. *IEEE Trans. Biomed. Eng.* **2013**, *60*, 3468–3483. [CrossRef]

40. Ribatti, D. Two new applications in the study of angiogenesis the CAM assay: Acellular scaffolds and organoids. *Microvasc. Res.* **2022**, *140*, 104304. [CrossRef]

41. Garreta, E.; Prado, P.; Tarantino, C.; Oria, R.; Fanlo, L.; Martí, E.; Zalvidea, D.; Trepat, X.; Roca-Cusachs, P.; Gavaldà-Navarro, A.; et al. Fine tuning the extracellular environment accelerates the derivation of kidney organoids from human pluripotent stem cells. *Nat. Mater.* **2019**, *18*, 397–405. [CrossRef]

42. Wörsdörfer, P.; Dalda, N.; Kern, A.; Krüger, S.; Wagner, N.; Kwok, C.K.; Henke, E.; Ergün, S. Generation of complex human organoid models including vascular networks by incorporation of mesodermal progenitor cells. *Sci. Rep.* **2019**, *9*, 15663. [CrossRef]

43. Hussein, N.A.; Mohamed, S.N.; Ahmed, M.A. Plasma ALU-247, ALU-115, and cfDNA Integrity as Diagnostic and Prognostic Biomarkers for Breast Cancer. *Appl. Biochem. Biotechnol.* **2019**, *187*, 1028–1045. [CrossRef]

44. Szmulewicz, M.N.; Novick, G.E.; Herrera, R.J. Effects of Alu insertions on gene function. *Electrophoresis* **1998**, *19*, 1260–1264. [CrossRef]

45. Wipper, S. *Validierung der Fluoreszenzangiographie für die Intraoperative Beurteilung und Quantifizierung der Myokardperfusion*; Ludwig-Maximilians-Universität München: München, Germany, 2006.

46. Umetani, N.; Giuliano, A.E.; Hiramatsu, S.H.; Amersi, F.; Nakagawa, T.; Martino, S.; Hoon, D.S.B. Prediction of breast tumor progression by integrity of free circulating DNA in serum. *J. Clin. Oncol.* **2006**, *24*, 4270–4276. [CrossRef]

47. Samorani, D.; Fogacci, T.; Panzini, I.; Frisoni, G.; Accardi, F.G.; Ricci, M.; Fabbri, E.; Nicoletti, S.; Flenghi, L.; Tamburini, E.; et al. The use of indocyanine green to detect sentinel nodes in breast cancer: A prospective study. *Eur. J. Surg. Oncol.* **2015**, *41*, 64–70. [CrossRef]

48. Hope-Ross, M.; Yannuzzi, L.A.; Gragoudas, E.S.; Guyer, D.R.; Slakter, J.S.; Sorenson, J.A.; Krupsky, S.; Orlock, D.A.; Puliafito, C.A. Adverse reactions due to indocyanine green. *Ophthalmology* **1994**, *101*, 529–533. [CrossRef]

49. Majlesara, A.; Golriz, M.; Hafezi, M.; Saffari, A.; Stenau, E.; Maier-Hein, L.; Müller-Stich, B.P.; Mehrabi, A. Indocyanine green fluorescence imaging in hepatobiliary surgery. *Photodiagn. Photodyn. Ther.* **2017**, *17*, 208–215. [CrossRef]

50. Baiocchi, G.L.; Diana, M.; Boni, L. Indocyanine green-based fluorescence imaging in visceral and hepatobiliary and pancreatic surgery: State of the art and future directions. *World J. Gastroenterol.* **2018**, *24*, 2921–2930. [CrossRef]

51. Neophytou, C.M.; Kyriakou, T.-C.; Papageorgis, P. Mechanisms of Metastatic Tumor Dormancy and Implications for Cancer Therapy. *Int. J. Mol. Sci.* **2019**, *20*, 6158. [CrossRef] [PubMed]

52. Rovithi, M.; Avan, A.; Funel, N.; Leon, L.G.; Gomez, V.E.; Wurdinger, T.; Griffioen, A.W.; Verheul, H.M.W.; Giovannetti, E. Development of bioluminescent chick chorioallantoic membrane (CAM) models for primary pancreatic cancer cells: A platform for drug testing. *Sci. Rep.* **2017**, *7*, 44686. [CrossRef] [PubMed]

53. Fry, L.C.; Mönkemüller, K.; Malfertheiner, P. Molecular markers of pancreatic cancer: Development and clinical relevance. *Langenbecks. Arch. Surg.* **2008**, *393*, 883–890. [CrossRef] [PubMed]

54. Cimpean, A.M.; Ribatti, D.; Raica, M. The chick embryo chorioallantoic membrane as a model to study tumor metastasis. *Angiogenesis* **2008**, *11*, 311–319. [CrossRef] [PubMed]

55. Feder, A.-L.; Pion, E.; Troebs, J.; Lenze, U.; Prantl, L.; Htwe, M.M.; Phyo, A.; Haerteis, S.; Aung, T. Extended analysis of intratumoral heterogeneity of primary osteosarcoma tissue using 3D-in-vivo-tumor-model. *Clin. Hemorheol. Microcirc.* **2020**, *76*, 133–141. [CrossRef] [PubMed]

56. Nakano, T.; Eckford, A.; Haraguchi, T. *Molecular Communication*; Cambridge University Press: Cambridge, UK, 2013; ISBN 978-1-107-02308-6.

57. Kuscu, M.; Unluturk, B.D. Internet of Bio-Nano Things: A review of applications, enabling technologies and key challenges. *ITU J. Future Evol. Technol.* **2021**, *2*, 1–24. [CrossRef]

58. Chahibi, Y. Molecular communication for drug delivery systems: A survey. *Nano Commun. Netw.* **2017**, *11*, 90–102. [CrossRef]

59. Lee, B.K.; Yun, Y.H.; Park, K. Smart Nanoparticles for Drug Delivery: Boundaries and Opportunities. *Chem. Eng. Sci.* **2015**, *125*, 158–164. [CrossRef]

60. Schafer, M.; Salinas, Y.; Ruderer, A.; Enzenhofer, F.; Bruggemann, O.; Martinez-Manez, R.; Rabenstein, R.; Schober, R.; Haselmayr, W. Channel Responses for the Molecule Release from Spherical Homogeneous Matrix Carriers. *IEEE Trans. Mol. Biol. Multi-Scale Commun.* **2022**, *8*, 212–228. [CrossRef]

61. Varzideh, F.; Pahlavan, S.; Ansari, H.; Halvaei, M.; Kostin, S.; Feiz, M.-S.; Latifi, H.; Aghdami, N.; Braun, T.; Baharvand, H. Human cardiomyocytes undergo enhanced maturation in embryonic stem cell-derived organoid transplants. *Biomaterials* **2019**, *192*, 537–550. [CrossRef]

62. Schmidt, S.; Alt, Y.; Deoghare, N.; Krüger, S.; Kern, A.; Rockel, A.F.; Wagner, N.; Ergün, S.; Wörsdörfer, P. A Blood Vessel Organoid Model Recapitulating Aspects of Vasculogenesis, Angiogenesis and Vessel Wall Maturation. *Organoids* **2022**, *1*, 41–53. [CrossRef]

63. Kaisto, S.; Saarela, U.; Dönges, L.; Raykhel, I.; Skovorodkin, I.; Vainio, S.J. Optimization of Renal Organoid and Organotypic Culture for Vascularization, Extended Development, and Improved Microscopy Imaging. *J. Vis. Exp.* **2020**. [CrossRef]

64. Lim, J.; Ching, H.; Yoon, J.-K.; Jeon, N.L.; Kim, Y. Microvascularized tumor organoids-on-chips: Advancing preclinical drug screening with pathophysiological relevance. *Nano Converg.* **2021**, *8*, 12. [CrossRef] [PubMed]
65. Sontheimer-Phelps, A.; Hassell, B.A.; Ingber, D.E. Modelling cancer in microfluidic human organs-on-chips. *Nat. Rev. Cancer* **2019**, *19*, 65–81. [CrossRef] [PubMed]
66. Fischer, D.; Fluegen, G.; Garcia, P.; Ghaffari-Tabrizi-Wizsy, N.; Gribaldo, L.; Huang, R.Y.-J.; Rasche, V.; Ribatti, D.; Rousset, X.; Pinto, M.T.; et al. The CAM Model-Q&A with Experts. *Cancers* **2022**, *15*, 191. [CrossRef]